Ion-bombardment-enhanced grain growth in germanium, silicon, and gold thin films

Harry A. Atwater,[a] Carl V. Thompson,[b] and Henry I. Smith[c]
Massachusetts Institute of Technology, Cambridge, Massachusetts 02139

(Received 22 January 1988; accepted for publication 22 May 1988)

Grain growth has been studied in polycrystalline thin films of Ge, Si, and Au during ion bombardment. The phenomenon has been characterized by varying the ion dose, ion energy, ion flux, ion species, substrate temperature, and thin-film deposition conditions. Films bombarded with Si^+, Ar^+, Ge^+, Kr^+, and Xe^+ exhibited enhanced grain growth which was weakly temperature dependent and proportional to the energy deposited in elastic collisions at or very near grain boundaries. The effect of these parameters on grain size and microstructure was analyzed both qualitatively and quantitatively using transmission electron microscopy. A transition state model describing the motion of grain boundaries during ion bombardment has been applied to the present experimental data. The results suggest that bombardment-enhanced grain growth may be due to thermal migration of bombardment-generated defects across the boundary. The calculated defect yield per incident ion was found to be directly related to enhanced grain growth, and was used to estimate the number of atomic jumps at the grain boundary per defect generated. Grain growth rates during bombardment and thermal annealing were related to their respective point defect populations.

I. INTRODUCTION

Ion-solid interactions have been the subject of intensive research in recent years, principally because ion beams are demonstrably useful for enhancing the kinetics of solid-phase processes, or making possible kinetic paths that are not accessible by thermal processes alone. This typically permits processing to be performed at temperatures much lower than those employed in conventional thermal processing. Grain growth has been extensively studied in metals and semiconductors, both in bulk and thin-film form. Recently, interest in thin-film grain growth has been renewed as polycrystalline materials are being employed in new applications in integrated circuits. The present grain growth study was motivated by the search for a low-temperature process for producing semiconductor-on-insulator thin films. More generally, study of ion-bombardment-enhanced grain-boundary motion may lead to further insight into the relationship between the structure and the properties of grain boundaries and other interfaces.

Ion-bombardment-enhanced grain growth has been studied in thin films of Ni,[1-3] Ge,[4,5] and Pd.[6] In Ni films bombarded with Ag^+ (Refs. 1 and 2) and Ge films bombarded with Ar^+, Ge^+, Kr^+, and Xe^+,[4,5] the grain growth rate was found to be proportional to the energy deposited in elastic collisions. For Ni (Ref. 3) and Pd,[6] it has been suggested that the maximum grain size is limited by the dimensions of the collision cascade generated by the incident ion.

In this paper, we describe the results of research on ion-bombardment-enhanced grain growth (IBEGG) in Ge, Au, and Si films. IBEGG has been characterized by varying the ion dose, ion energy, ion flux, ion species, temperature, and thin-film deposition conditions. The effects of these parameters on grain size and microstructure have been analyzed using transmission electron microscopy and transmission electron diffraction. Samples were examined in both plan-view and cross-sectional configurations. A model that describes the motion of grain boundaries during ion bombardment has been developed, and is in good agreement with the experimental results.

II. EXPERIMENT

In the research described here, we have focused on normal grain growth in films in which both the initial and final grain sizes were less than or equal to the film thickness. The term normal grain growth refers to growth which is driven by the reduction of grain-boundary energy, and which is characterized by a monomodal grain size distribution whose average size increases continuously with time. Normal grain size distributions are found to be approximately lognormal in both films[7] and bulk samples,[8] but other forms for the distribution are predicted by existing theories.[9,10] It has been found experimentally that normal grain growth slows down rapidly once grains have grown to sizes comparable to the film thickness.[7] It is possible that surface grooving of grain boundaries is responsible for the slowing of normal grain growth.[11]

In the research described here, we have investigated grain growth starting with grain sizes smaller than the film thickness and ending once a columnar structure develops, i.e., when all grain boundaries extend from the top to the bottom surfaces of the films. Ion energies were varied 40 to 200 keV, and were chosen so that the peak of the ion damage profile was approximately in the middle of the film, as depicted in Fig. 1. The thin films were either unsupported (to facilitate TEM observation) or deposited on thermally grown SiO_2 substrates. The film thickness was chosen to be comparable to the standard deviation of the ion damage pro-

[a] Current address: Thomas J. Watson Sr. Laboratory of Applied Physics, California Institute of Technology, Pasadena, CA 91125.
[b] Department of Materials Science and Engineering.
[c] Department of Electrical Engineering and Computer Science.

 0021-8979/88/172337-17$02.40

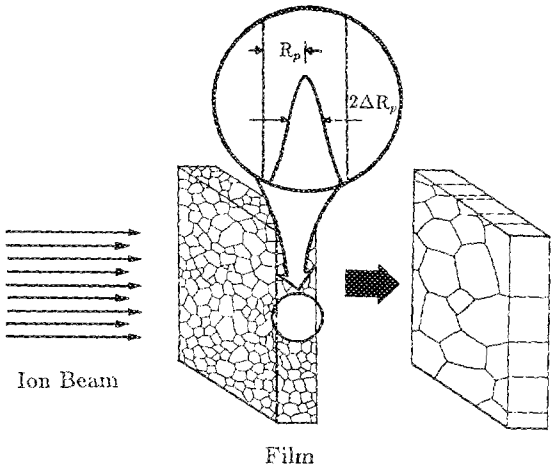

FIG. 1. Schematic of the IBEGG process showing the development of a columnar grain structure.

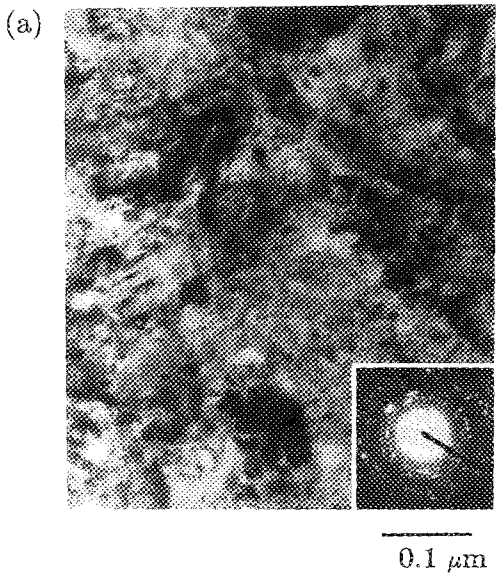

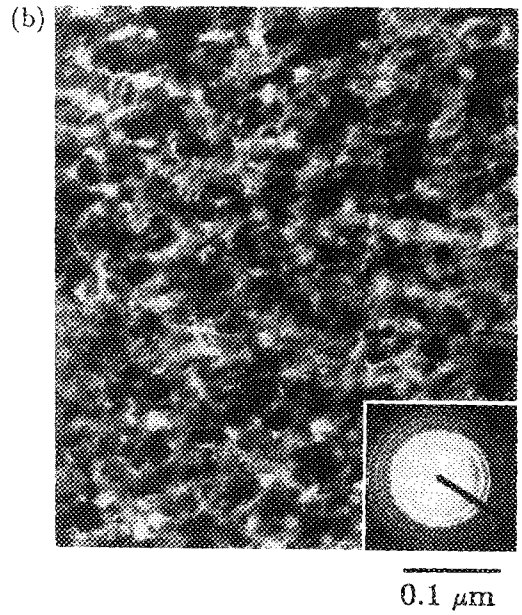

FIG. 2. (a) Transmission electron micrograph and transmission electron diffraction pattern for amorphous as-deposited Ge film on thermal SiO_2 after crystallization are shown. (b) Transmission electron micrograph and transmission electron diffraction pattern for polycrystalline as-deposited Ge film on thermal SiO_2 after deposition at 400 °C.

file. This film thickness regime is the one in which secondary grain growth has been observed in thermal annealing experiments in all three materials.[7,12–14]

During IBEGG, the substrate was maintained at a temperature sufficiently high for annealing of ion damage as IBEGG proceeded. For Ge this temperature ranged from 450 to 700 °C, and for Si from 700 to 1050 °C. In Au films, room temperature was sufficient for annealing of ion damage during bombardment.

A. Thin-film deposition

Thin germanium films were prepared in three ways. In the first, films were formed by room-temperature electron beam evaporation of Ge onto clean thermally grown SiO_2-on-Si substrates. The substrates were cleaned in a 1:1:5 mixture of H_2O_2, NH_4OH, and H_2O at 80 °C, and were either immediately loaded into the evaporation chamber or stored under rough vacuum until being loaded. The SiO_2 was grown by a dry oxidation process at 1050 °C on (100) Si wafers, and the thickness ranged from 910 to 1150 Å, as measured using an ellipsometer. The Ge films, deposited at 10 Å/s, were amorphous as-deposited, and were crystallized while being heated to the temperature for ion-bombardment-enhanced grain growth, as shown in Fig. 2(a). The crystallographic texture of these films appeared to be random.

A second set of Ge films were prepared by deposition onto clean thermally grown SiO_2-on-Si substrates at a temperature of 400 °C. These samples were found to be polycrystalline, as shown in Fig. 2(b). These films appeared to have random polycrystalline texture. The polycrystalline as-deposited films exhibited a columnar morphology with grain widths smaller than the film thickness, while the amorphous-deposited films that were subsequently crystallized were noncolumnar. This is shown in the cross-sectional transmission electron micrographs of Figs. 3(a) and 3(b).

Unsupported (freestanding) films of Ge were formed by room-temperature electron beam evaporation of Ge onto freshly cleaved NaCl substrates. The evaporation rate was 10 Å/s. These films were floated off the NaCl substrates onto TEM grids in deionized water (DI-H_2O). These samples were amorphous as-deposited, as indicated by transmission electron diffraction. The Ge films underwent crystallization while being heated to the temperature for ion-bombardment-enhanced grain growth. The crystallized films appeared to have a random polycrystalline texture, as indicated by transmission electron diffraction.

Gold films were deposited onto cleaned SiO_2 substrates by room-temperature electron beam evaporation, at a rate of 10 Å/s. Some of the films were 250 Å thick, and others were 500 Å thick. The films were then floated off the SiO_2 onto TEM grids using DI-H_2O as soon as possible after depo-

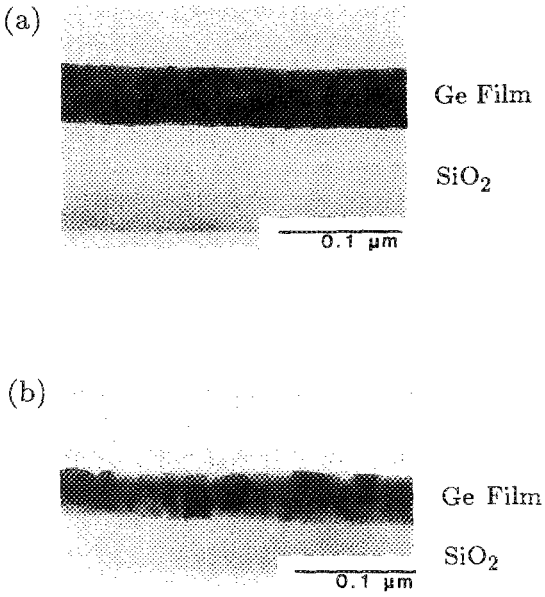

FIG. 3. Cross-sectional electron micrographs of (a) an amorphous as-deposited Ge film after crystallization and (b) a polycrystalline as-deposited Ge film.

sition. Typically, the time was 10 min. Gold films are polycrystalline when deposited at room temperature, as seen in Fig. 4. The crystallographic texture in the as-deposited films appeared to be random. Grain growth in thin gold films occurs readily at room temperature on SiO_2 substrates, but it virtually stops in films that have been rendered freestanding.[12] In order to prevent confusion between thermal and ion-bombardment-enhanced grain growth, freestanding

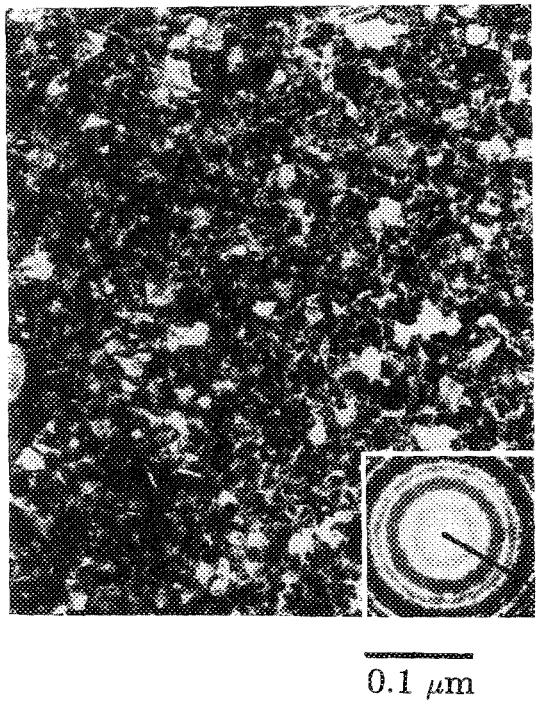

FIG. 4. Transmission electron micrograph and transmission electron diffraction pattern for polycrystalline as-deposited Au film, deposited on thermal SiO_2 substrate and after removal from the substrate.

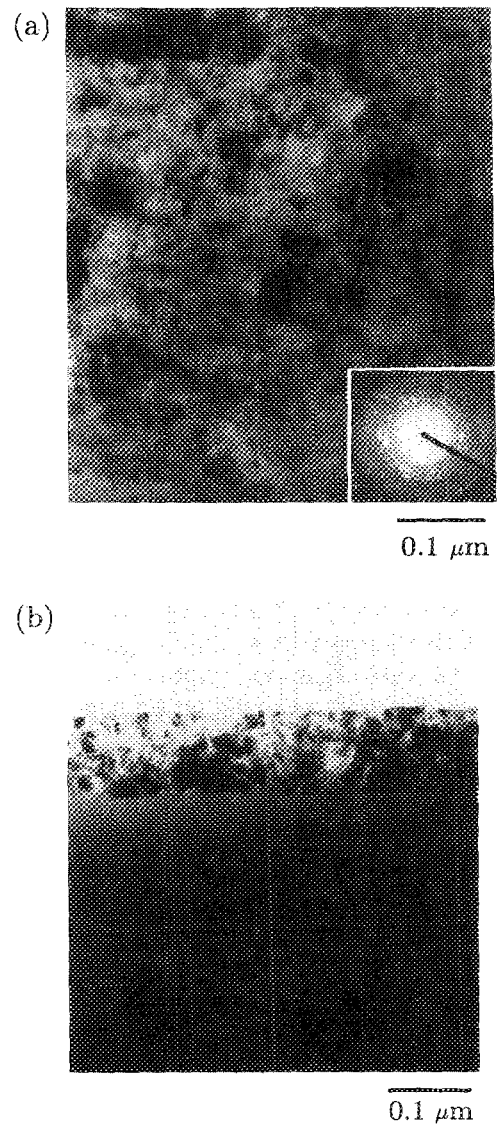

FIG. 5. (a) Transmission electron micrograph and transmission electron diffraction pattern for amorphous as-deposited Si film on thermal SiO_2 after crystallization. (b) Cross-sectional electron micrographs of an amorphous as-deposited 1000-Å-thick Si film on SiO_2 after crystallization.

gold films were exclusively used in the experiments described here.

Silicon films were deposited on thermally grown SiO_2 by room-temperature electron beam evaporation, at a deposition of 1 Å/s. As with Ge films, the Si films were crystallized while being heated to the temperature for ion-bombardment-enhanced grain growth. These films also appeared to exhibit random polycrystalline texture. All Si films were 1000 Å thick, unless otherwise noted. Figure 5(a) shows the amorphous as-deposited film after crystallization. In Fig. 5(b), a cross-sectional view of the as-deposited film is shown.

B. Thermal annealing

The samples that were subjected to thermal annealing were placed in quartz ampoules which were evacuated to approximately 10^{-7} Torr using a turbomolecular pump.

The ampoules were then sealed under vacuum and annealed in a furnace held at constant temperature. After deposition and prior to annealing, silicon samples were cleaned in a 1:1:5 solution of H_2O_2, NH_4OH, and H_2O. The germanium samples were cleaned by exposure to deep ultraviolet radiation in air. This creates ozone and atomic oxygen which removes residual organic contaminants.[15] Several wet chemical cleaning approaches similar to the standard clean were tried, but were not used because they resulted in removal of the germanium film. The Au films were also cleaned using ultraviolet irradiation prior to grain growth.

C. Ion bombardment

The projectile ions were chosen to be either native species (i.e., Ge^+ in Ge) or noble gases in order to avoid confusion between physical and chemical kinetic enhancement, such as dopant-enhanced boundary migration.[13,16–18] In all cases, the base pressure in the implantation chamber was between 5×10^{-7} and 1×10^{-6} Torr. Source gas purity was in the ppm range, and mass separation was used to generate a single species beam. Silicon and germanium beams were generated by creating a discharge in silane or germane gas. Beams of Ar^+, Kr^+, and Xe^+ were generated using research purity sources.

Samples were mounted on a 1.6-mm-thick resistively heated graphite strip. Temperature measurements were made with 0.2-mm wire chromel-alumel thermocouples embedded within the graphite strip. Between 650 and 900 °C, the thermocouple readings were compared with measurements made using a disappearing filament-type optical pyrometer. The pyrometric temperature measurements were calibrated against similar measurements made with Si substrates annealed under vacuum in a furnace at constant temperature.

Power was supplied to the graphite strip using a silicon-controlled rectifier (SCR) power controller, through a 20:1 voltage step-down transformer. A microprocessor controller was programmed to receive the temperature measurement from the thermocouple and control the power delivered to the graphite strip by the power controller. This feedback system maintained a constant temperature within $\pm$ 5 °C. From pyrometric measurements, the Si substrate material was found to be approximately 50 °C lower than the stage temperature measured by the thermocouples. For temperatures lower than 650 °C, which could not be probed by the optical pyrometer, the substrate temperature was assumed also to be approximately 50 °C lower than the stage temperature.

D. Analysis

The film microstructure and crystallographic orientation were characterized by transmission electron microscopy (TEM) and transmission electron diffraction (TED). The grain size and morphology were examined by bright- and dark-field TEM. The grains imaged in bright- and dark-field micrographs were digitized to facilitate computer generation of grain size distributions. The recorded grain sizes were the maximum in-plane dimension of grain sizes in the micrographs. The micrographs were photographically enlarged so that the grain size on the printed micrograph was large compared to the measurement error in the digitizing process. Because individual grains in a film with noncolumnar structure are difficult to resolve in bright field, grain size measurements in the noncolumnar films were taken from dark-field micrographs. Grain size measurements in the columnar films were derived from both bright- and dark-field micrographs, which gave identical results. Grain size data were fitted to lognormal distributions. The experimental distributions were approximately lognormal for all the experiments conducted in this work. This is consistent with previous observation of grain size distributions in normal grain growth.[7,8]

The TRIM Monte-Carlo simulation program[19] was used for various ion transport calculations, including determination of the projected range of implanted ions, and the Frenkel defect yield per incident ion as deduced from a modified Kinchin Pease algorithm.[20] For Si and Ge, a displacement energy of 15 eV was used, while for Au an energy of 25 eV was assumed. For each case, the program was run until statistical fluctuations in the projected range and defect yield were less than 3%. This usually required histories of 100–300 ions per simulation. Computer calculations have been able to predict experimental ion range distributions very successfully.[21] However, there is at present no experimental technique which can allow definitive measurement of the nuclear energy loss or defect yield per incident ion. Electron microscopy studies to measure the defect yields have been performed,[22] but the results of such studies are almost always questionable. This is because thermal defect annealing causes an underestimation of the defect population, even when bombardment is carried out at low temperatures. Nonetheless, it is assumed in this work that the TRIM calculations of defect generation produce reasonably accurate results.

III. RESULTS AND DISCUSSION

A. Germanium films

While normal grain growth during thermal annealing of Si and Au films has been previously investigated,[12,16,18] data for normal grain growth of unencapsulated Ge films in the regime of interest here did not exist. Hence, measurements of thermally induced grain-boundary migration in Ge were undertaken, and are described first. The variation of grain size with time in an unencapsulated, 500-Å-thick, amorphous as-deposited Ge film during thermal annealing at $T = 775$ °C is shown in Fig. 6. The data indicate that

$$r \propto t^{0.28}, \tag{1}$$

where the grain radius is r, and t is time. This is consistent with the experimentally observed time dependence in metals[23,24] and ceramics,[25,26] but is inconsistent with existing theories for normal grain growth.[8–10]

The variation of the grain growth rate with temperature in 500-Å-thick, thermally annealed Ge films is shown in Fig. 7. Data were taken between 750 and 815 °C. Below 750 °C, grain growth was not observed in a convenient time interval, and above 815 °C, beading of the film prevented observation

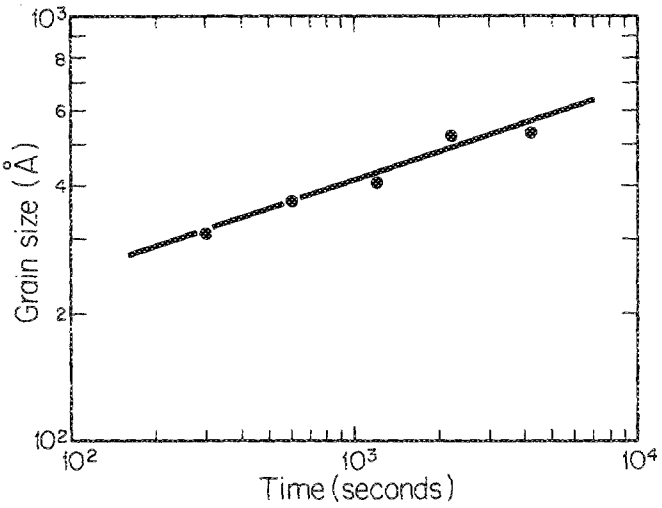

FIG. 6. Time dependence of grain growth in amorphous-deposited Ge films for thermal annealing at 775 °C.

of grain growth. The indicated growth rate was determined at one half of the final grain size. Thus the driving force due to grain boundary energy, which is inversely proportional to the grain size, was assumed to be constant. Using a simple model for normal grain growth, the activation energy for grain growth is estimated to be $E_a = 2.7 \pm 0.7$ eV. This measurement indicates that the activation energy for thermal grain-boundary motion is between two thirds of and approximately equal to the activation energy for self-diffusion, 3.1 eV.[27]

The electron micrographs in Fig. 8 illustrate the morphology of a freestanding Ge film which has undergone ion-bombardment-enhanced grain growth at 600 °C.[5] A 50 keV Ge^+ beam was used, with a current density of 1.56×10^{12} ions/cm^2 s. Figure 8(a) is an electron micrograph of a film implanted with an ion dose of 5×10^{13}/cm^2. The average grain size is approximately 100 Å and the microstructure is noncolumnar. Close inspection reveals a high density of dislocations within grains. Figure 8(b) is a similar micrograph of a film implanted with an ion dose of 5×10^{14}/cm^2, and

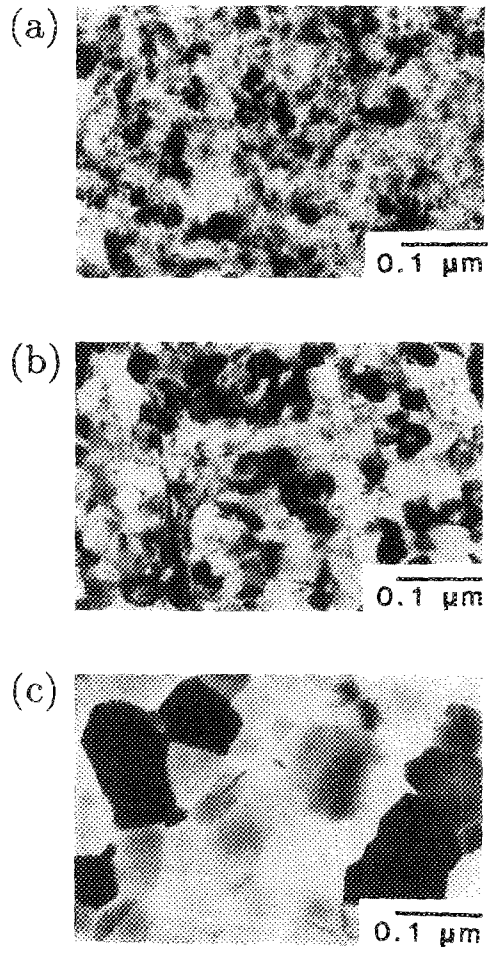

FIG. 8. Transmission electron micrographs of a freestanding 500-Å-thick Ge film at 600 °C implanted with 50 keV Ge^+ at a dose of (a) 5×10^{13}/cm^2, (b) 5×10^{14}/cm^2, (c) 5×10^{15}/cm^2.

Fig. 8(c) is a film implanted with an ion dose of 5×10^{15}/cm^2. The increase in grain size in Figs. 8(b) and 8(c) is apparent, and the change in morphology with increasing grain size is consistent with our understanding that normal grain growth is driven by a reduction in grain-boundary en-

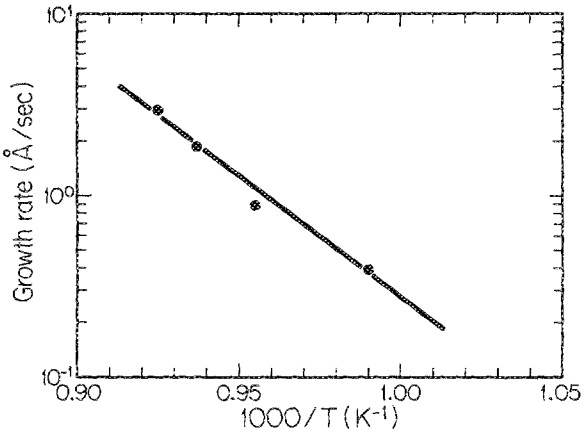

FIG. 7. Temperature dependence of grain growth rate in Ge films during thermal annealing at grain size equal to one half the final grain size.

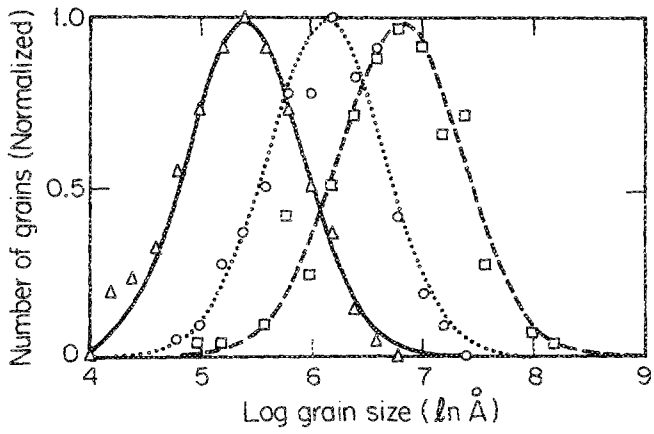

FIG. 9. Lognormal grain size distributions for IBEGG with 50 keV Ge^+ at doses of 5×10^{13}/cm^2, 5×10^{14}/cm^2, and 5×10^{15}/cm^2.

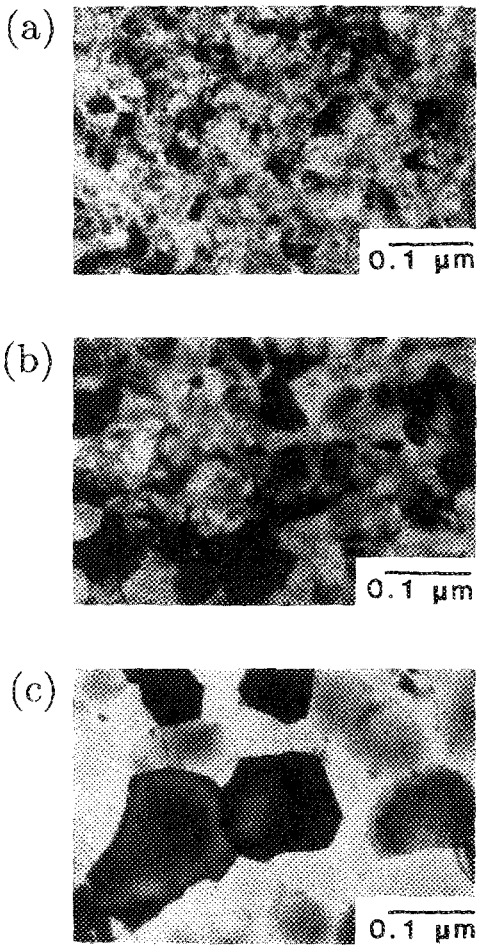

FIG. 10. Transmission electron micrographs of a freestanding 500-Å-thick Ge film at 500 °C implanted with 50 keV Ge^+ at a dose of (a) $5\times10^{13}/cm^2$, (b) $5\times10^{14}/cm^2$, (c) $5\times10^{15}/cm^2$.

ergy. That is, as the grain size increases the grain-boundary curvature is reduced. Boundary curvature normal to the plane of the film is reduced as the film develops a columnar grain structure. The grain size distributions corresponding to the micrographs of Fig. 8 are shown in Fig. 9. Note that the distributions are also lognormal, and that the peak of the lognormal distributions move to larger grain sizes with increasing ion dose.

Figure 10 illustrates the morphology and change in grain size for a freestanding Ge film which has undergone ion-bombardment-enhanced grain growth at 500 °C. As in the previous case, a 50 keV Ge^+ beam was used, with a current density of 1.56×10^{12} ions/cm^2 s. The variation of grain size and microstructure is qualitatively very similar to that seen at 600 °C. The grain size increase and development of a columnar structure is similar over the same range of ion doses. This suggests that ion-beam-enhanced grain growth is only very weakly temperature dependent.

Figure 11 shows cross-sectional electron micrographs of 500-Å-thick Ge films on 1000 Å of thermally grown SiO_2 after IBEGG at 600 °C with a 50 keV Ge^+ beam at doses of $5\times10^{13}/cm^2$ and $5\times10^{15}/cm^2$. The micrograph in Fig. 11(a) confirms the noncolumnar microstructure of the film at the initial stages of normal grain growth. The micrograph

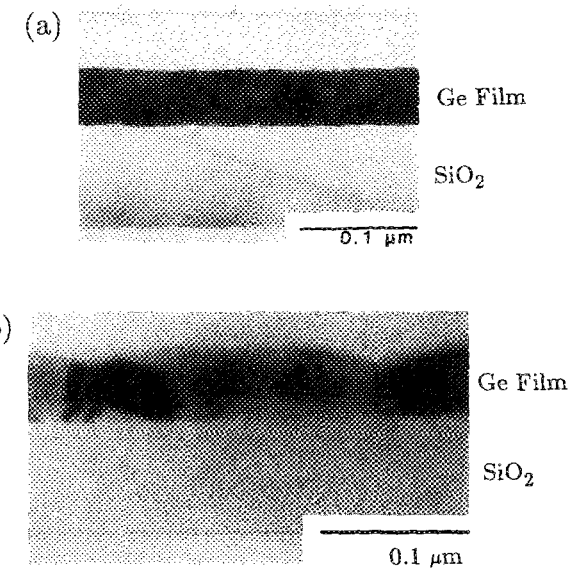

FIG. 11. Cross-sectional electron micrograph of 500-Å-thick Ge film after IBEGG at 600 °C with a 50 keV Ge^+ beam at a dose of (a) $5\times10^{13}/cm^2$ and (b) $5\times10^{15}/cm^2$. Note the grain-boundary grooves in (b).

in Fig. 11(b) indicates that the film has developed a columnar structure and that there are deep grooves at the grain boundaries. These grooves certainly influence the driving force for growth and may be responsible for the slowing down of grain growth as the grain size approaches the film thickness.[11]

The dependence of grain size on ion dose for a variety of Ge films deposited in amorphous and polycrystalline form is shown in Fig. 12. Results are shown for both unsupported films and films on thermal SiO_2 substrates. The change of the

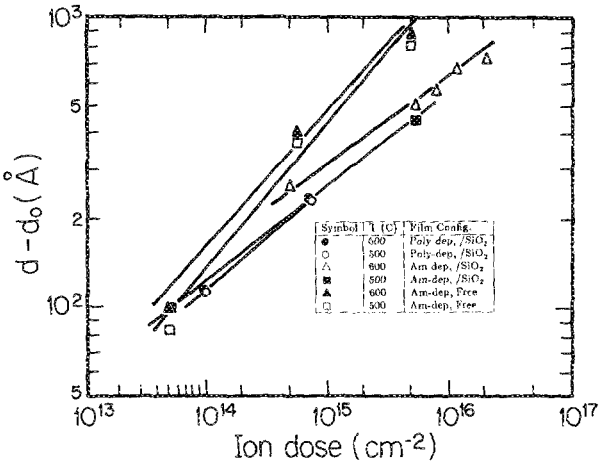

FIG. 12. Variation of grain size with ion dose for various 500 Å Ge films bombarded with 50 keV Ge^+. Closed circles are data for polycrystalline as-deposited films on SiO_2 bombarded at 600 °C; open circles are for polycrystalline as-deposited films on SiO_2 bombarded at 500 °C; open triangles are for amorphous as-deposited on SiO_2 substrates bombarded at 600 °C; closed triangles are for unsupported amorphous as-deposited bombarded at 600 °C; closed squares are for amorphous as-deposited on SiO_2 substrates bombarded at 500 °C; open squares are for unsupported amorphous as-deposited bombarded at 500 °C.

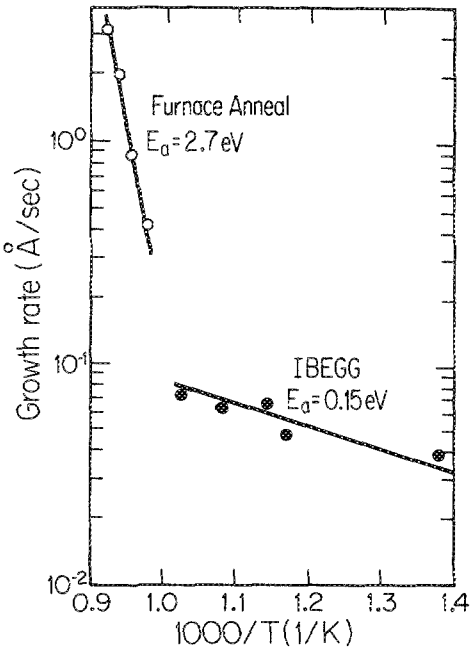

FIG. 13. Arrhenius plot of growth rate at one half the final grain size of Ge for thermal annealing and ion-bombardment-enhanced grain growth at a constant flux of 1.5×10^{12} ions/cm^2 s.

average grain diameter with ion dose $(d-d_0)$ is similar for all substrates and deposition conditions, suggesting that the basic mechanism of IBEGG is similar in these various experiments. At a constant ion flux, the dose dependence is equivalent to a time dependence for grain growth. The time dependence varies from $r\propto t^{0.25}$ for the polycrystalline as-deposited films to $r\propto t^{0.31}$ for amorphous as-deposited free-standing films. These growth exponents fall within the range of experimentally observed growth exponents in other systems,[23–26] and in the thermal annealing experiments described above. The difference in growth exponents may be related to microstructural differences in the various films. For example, the polycrystalline as-deposited films, which

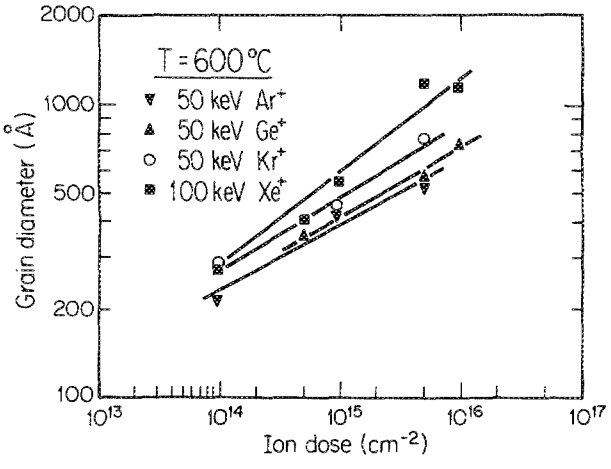

FIG. 14. Variation of grain size with ion dose for 500-Å-thick Ge films on SiO_2 implanted with Ar^+, Ge^+, Kr^+, and Xe^+ ions, all at 600 °C.

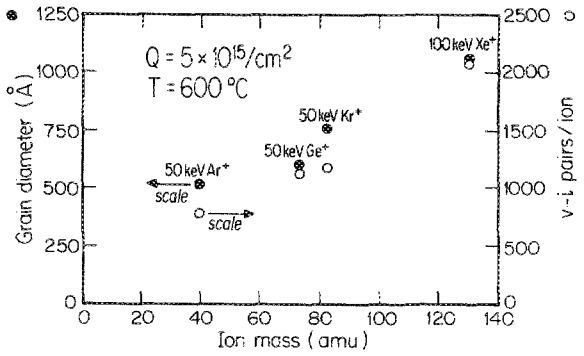

FIG. 15. Comparison of grain size and the number of defects generated per incident ion with projectile ion mass at 600 °C. The ion dose was 5×10^{15}/cm^2 for all cases. Closed circles refer to the left ordinate, and open circles refer to the right ordinate.

have the smallest growth exponent, presumably have a smaller driving force than the amorphous as-deposited films, owing to their approximately columnar microstructure before grain growth (see Fig. 3). The greatly reduced curvature of grain boundaries normal to the plane of the film results in a lower driving force at a given grain size. In general, the variation of IBEGG with time is similar to the observed time dependence for thermal grain growth, which suggests that atomic processes which occur at grain boundaries are rate limiting in both cases.

The temperature dependence of the grain growth rate in 500-Å-thick amorphous as-deposited Ge films which have undergone ion-beam-enhanced grain growth during bombardment with 50 keV Ge^+ between 450 and 700 °C is shown in Fig. 13. This is to be compared with the temperature dependence of similar films which have been thermally annealed. As previously mentioned, the thermal data indicate an activation energy for grain-boundary motion of approximately 2.7 eV. Unlike thermal annealing, IBEGG is characterized by a very weak temperature dependence. The measured activation energy of 0.15 eV for the IBEGG process is lower than measured energies for vacancy migration in Ge (Ref. 27) and Si.[28]

Ion-bombardment-enhanced grain growth in Ge has also been studied using various projectile ion species. Figure 14 depicts the variation of grain diameter with ion dose for 50 keV Ar^+, 50 keV Kr^+, 50 keV Ge^+, and 100 keV Xe^+ ions incident on 500-Å-thick amorphous as-deposited Ge films at 600 °C. The form of the time dependence for grain growth is similar for all projectile ions. However, the grain size for a given ion dose increases with increasing projectile ion mass. Figure 15 depicts the variation of grain size in amorphous as-deposited Ge films at 600 °C with incident ion mass, at a constant dose of 5×10^{15}/cm^2. Also shown is the number of vacancy-interstitial pairs created per incident ion at the given energy calculated using the TRIM code. A close correlation is seen between the number of vacancy-interstitial pairs produced per incident ion and the increase in grain size. This result suggests that the defects responsible for IBEGG can be described using linear collision cascade theory.

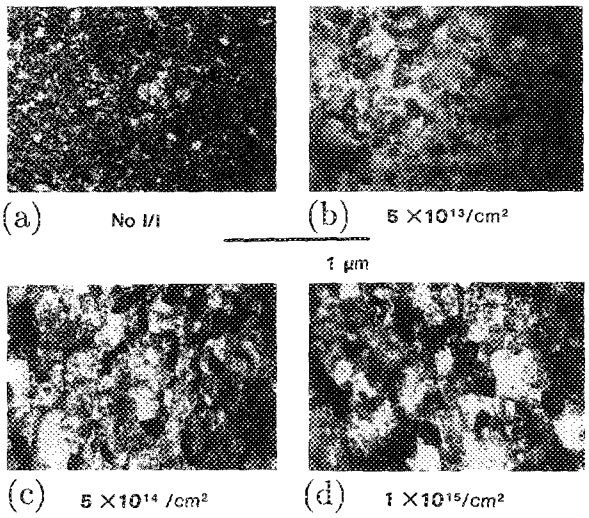

FIG. 16. Transmission electron micrographs of a 250 Å Au film after IBEGG with a 200 keV Xe^+ beam, with an ion flux density of 1.5×10^{13}/cm^2 s. In (a) no implant, (b) 5×10^{13}/cm^2, (c) 5×10^{14}/cm^2, (d) 1×10^{15}/cm^2.

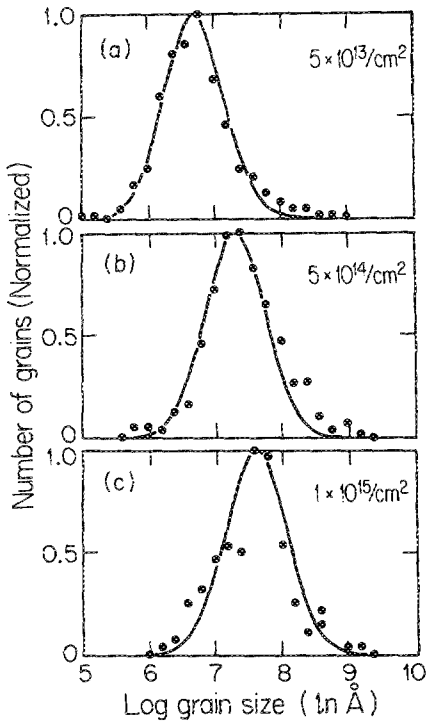

FIG. 17. Grain size distributions for a 250 Å Au film after IBEGG with a 200 keV Xe^+ beam, with an ion flux density of 1.5×10^{13}/cm^2 s. In (a) 5×10^{13}/cm^2, (b) 5×10^{14}/cm^2, (c) 1×10^{15}/cm^2.

B. Gold films

The morphology of 250-Å-thick Au films which have undergone IBEGG is shown in Fig. 16. Films 500 Å thick exhibited a similar increase in grain size. A 200 keV Xe^+ beam with a current density of 1.5×10^{13}/cm^2/s was employed, and the substrate temperature was room temperature (23 °C). The 250-Å-thick unimplanted film is characterized by a noncolumnar grain structure with grain sizes smaller than the film thickness. A dose of 5×10^{13}/cm^2 caused a columnar grain structure to develop, as seen in Fig. 16(b). Higher doses [Figs. 16(c) and 16(d)] result in further grain growth. However, unlike Ge, the density of defects within grains increases with increasing ion dose. Impurity-related defects in the films could not be detected using energy dispersive x-ray analysis in a scanning transmission electron microscope.

An important question to consider in the study of IBEGG in gold films is whether the process is one of secondary grain growth or normal grain growth. Surface energy driven secondary grain growth is characterized by evolution of a bimodal grain size distribution and the development of a strong crystallographic texture.[14] Both of these attributes have been found in grain growth in thin Au films which have undergone thermal grain growth at room temperaure.[12]

Grain size distributions for ion-bombarded 250-Å-thick Au films are shown in Fig. 17. These distributions correspond to the electron micrographs of Fig. 16. The distributions are monomodal and approximately lognormal. During IBEGG the peaks of the distributions move to larger grain sizes. The monomodal character of the distributions tends to support a view of IBEGG in 250-Å Au films as being a normal grain growth process. However, it is an unusual normal grain growth process, since the grain size is apparently not limited by the specimen thickness.

Although the monomodality of the grain size distributions is consistent with normal grain growth, the change of crystallographic texture as a result of IBEGG may indicate that surface energy plays a role in grain growth. The electron diffraction patterns for 250-Å films bombarded with 1×10^{15}/cm^2 Xe^+ at 200 keV exhibited {200}, {222}, and {111} rings which were greatly reduced in intensity, as compared with an unbombarded film. The {220} ring, corresponding to (111) texture, increased in intensity as a result of bombardment.

Taken together, the observations of the grain size distributions and crystallographic texture in Au films during IBEGG point to a grain growth process in which *both grain-boundary energy and surface energy play a role*. The observed monomodal grain size distributions may imply that surface energy is not the predominant driving force. However, the change in crystallographic texture indicates that it is not negligible either.

It has been proposed that ion channeling can play a role in the development of film texture[29] during grain growth. In the experiments described here, it is possible that the incident ion beam was at least partially channeled in certain well-oriented grains. However, channeling does not seem to have played a role in selectively promoting grain growth, since (111) texture is not consistent with beam alignment with the optimum channeling direction.

The dose dependence for IBEGG in thin Au films bombarded with 200 keV Xe^+ ions is shown in Fig. 18. Grain sizes increased with ion dose for both 250- and 500-Å-thick films with a time dependence given by

$$r(t) \propto t^{0.3} \qquad (2)$$

in both cases. This is consistent with the results for Ge dis-

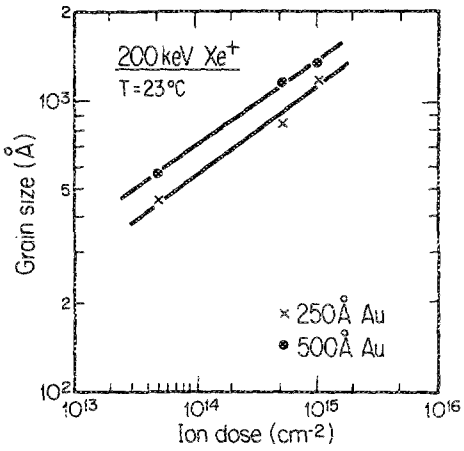

FIG. 18. Variation of grain size with ion dose in Au films bombarded by 200 keV Xe^+ with an ion flux density of $1.5\times10^{12}/cm^2$ s at 23 °C.

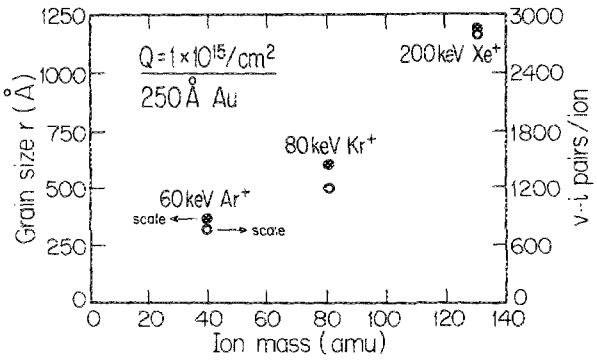

FIG. 20. Comparison of grain size and the number of defects generated per incident ion with projectile ion mass during IBEGG in 250 Å Au films at room temperature. The ion dose was $1\times10^{15}/cm^2$ for all cases. Closed circles refer to the left ordinate, and open circles refer to the right ordinate.

cussed above and other investigations of normal grain growth. The dependence of grain size with time for IBEGG with 80 keV Kr^+ and 200 keV Xe^+ ions is shown in Fig. 19. The time dependence is the same for both species, which is similar to the observations made for Ge films, implying that the grain growth process is similar in both cases.

Figure 20 depicts the variation in grain size in 250-Å-thick Au films with incident ion mass, at a constant dose of $1\times10^{15}/cm^2$. Also shown is the number of vacancy-interstitial pairs per incident ion at the given energy, calculated using the TRIM code. A close correlation is seen between the number of vacancy-interstitial pairs produced per incident ion and the increase in grain size. This result, similar to that obtained for Ge films, again suggests that the defects responsible for IBEGG in Au films can be described using linear collision cascade theory and the Kinchin–Pease formalism.

The variation of grain size with incident ion energy in 250-Å-thick Au films bombarded by $1\times10^{15}/cm^2$ of Kr^+ is shown in Fig. 21. The grain size increases with increasing ion energy in an approximately linear fashion. Also plotted is the number of defects produced/incident ion, as calculated using the TRIM code. A reasonable correlation is observed between the calculated defect yield and the grain size, a result which is in agreement with the Kinchin–Pease model for defect production and the model proposed for IBEGG.

An important consideration in the characterization of IBEGG is to assess the role of heating of the film by the ion beam. If heating of the film by the ion beam leads to thermal grain growth, the effect should be detectable by monitoring grain growth for different ion fluxes. Figure 22 illustrates the time dependence of grain growth during 200 keV Xe^+ bombardment for two different ion fluxes, 1.5×10^{12} and 1.5×10^{13} ions/cm^2 s. The data indicate that increasing the ion flux by a factor of 10 simply increases the growth rate by a factor of 10. Said another way: the grain size is a function of the ion dose, not the ion flux. This finding indicates that thermal annealing of the film is negligible.

Another test for the possibility of ion beam heating was employed. By masking part of the film from the beam, contiguous regions which were either bombarded or not bombarded could be studied. If ion beam heating were to influence grain growth in the bombarded region, presumably the unbombarded region would also experience growth due to heating by conduction. The transmission electron micrograph of Fig. 23 illustrates the border between a bombarded and an unbombarded region in a 500-Å-thick Au film bombarded with 200 keV Xe^+ with a flux of $1.5\times10^{13}/cm^2$ s and a dose of $1\times10^{15}/cm^2$. Small noncolumnar grains are seen in the unbombarded region, and larger grains are seen in the

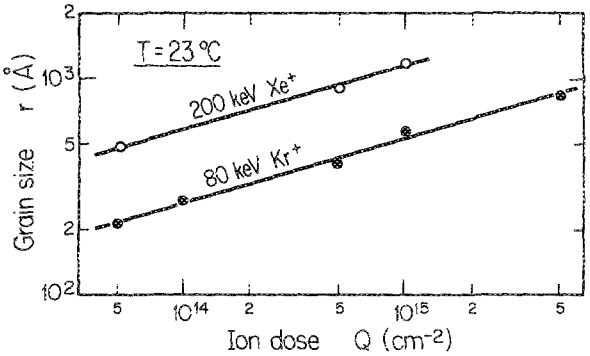

FIG. 19. Variation of grain size with time for 80 keV Kr^+ and 200 keV Xe^+ ions incident on a 250 Å Au film.

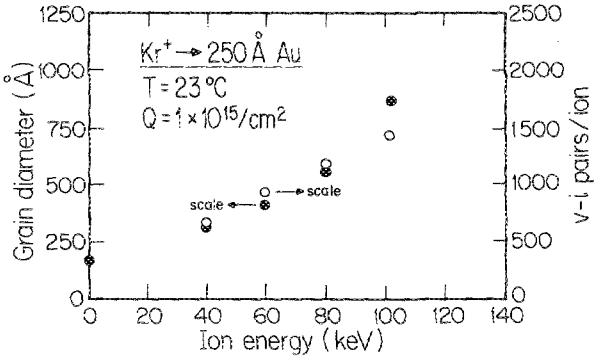

FIG. 21. Variation of grain size with ion energy during IBEGG using a flux of $1.5\times10^{12}/cm^2$ s. The dose was held constant at $1\times10^{15}/cm^2$.

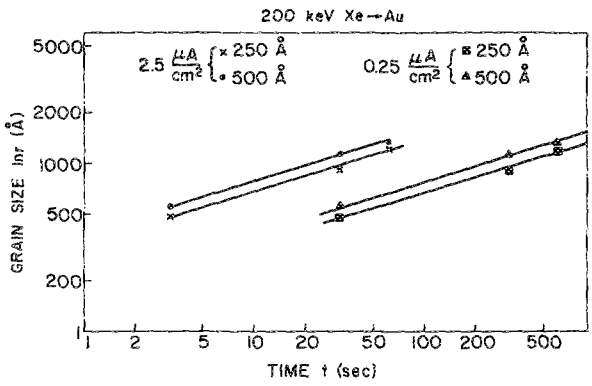

FIG. 22. Variation of grain size with time for two different ion fluxes.

bombardment region. The demarcation between the two regions approximately corresponds to the lateral straggle of the ion beam. This result supports a model of grain growth in which only those regions which experience elastic collisions undergo grain growth. The lack of grain growth in the unbombarded region is interpreted as evidence for a lack of ion beam heating of this area. Similar conclusions were obtained in a study of bombardment-enhanced growth of Ni films.[2]

C. Silicon films

The microstructure of a silicon film after IBEGG is shown in Fig. 24. A 1000-Å-thick Si film was bombarded with 150 keV Xe^+ ions at a current density of 1.8×10^{12}/cm^2 s, and at a substrate temperature of 850 °C. The film

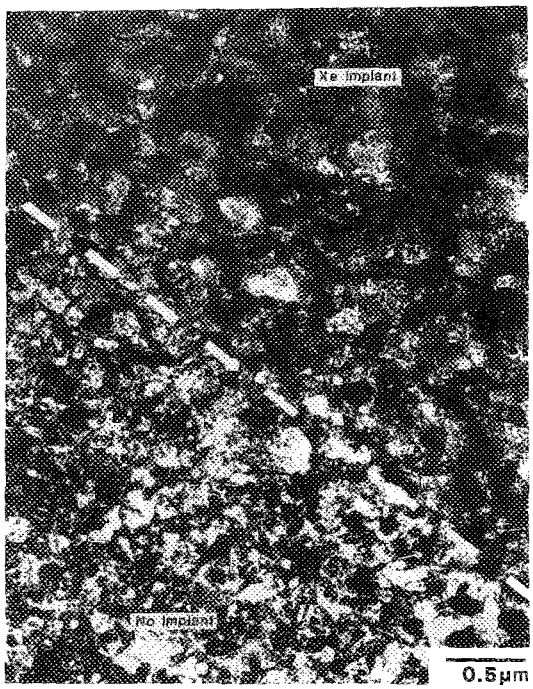

FIG. 23. A 500 Å Au film which has been partially masked from exposure to a 200 keV Xe^+ beam. The transmission electron micrograph illustrates the sharp delineation between the enhanced growth region which has been bombarded, and the unbombarded region which experienced no enhanced grain growth.

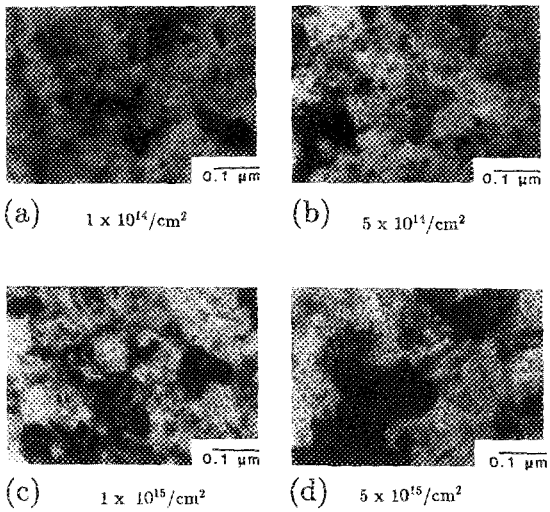

FIG. 24. Microstructure of a 1000-Å-thick Si film after IBEGG at 850 °C with 150 keV Xe^+ for various ion doses. In (a), 1×10^{14}/cm^2; in (b), 5×10^{14}/cm^2; in (c), 1×10^{15}/cm^2; and in (d) 5×10^{15}/cm^2.

surface was inclined at an angle of 45° to the ion beam. In Figs. 24(a) and 24(b), a noncolumnar grain structure is seen for films bombarded with 1 and 5×10^{14}/cm^2, respectively. At a dose of 1×10^{15}/cm^2, some grain growth is seen, and a dose of 5×10^{15} results in further grain growth as seen in Figs. 24(c) and 24(d).

At the highest dose studied here, the grain structure was not columnar. Cross-sectional TEM revealed that enhanced grain growth took place only within the top two thirds of the 1000-Å Si film, which is consistent with estimates of the position of the damage profile as indicated in Fig. 25(a). The fact that the grain size was not uniform normal to the plane

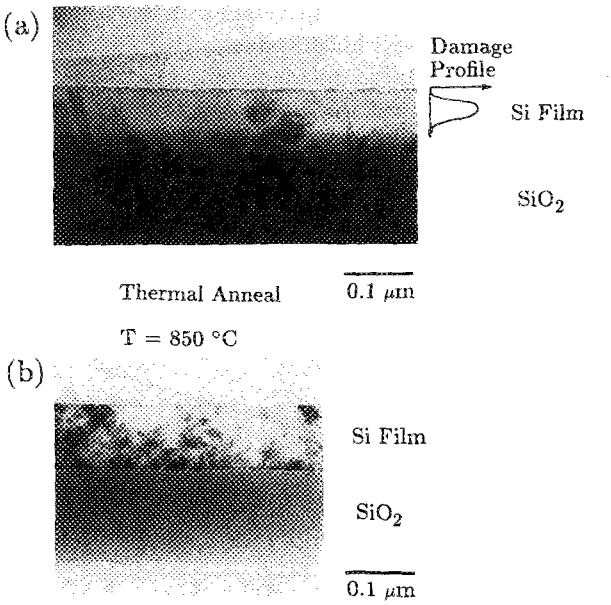

FIG. 25. In (a), cross-sectional electron micrograph of a 1000 Å Si film after IBEGG at 850 °C with a 150 keV Xe^+ beam at a dose of 5×10^{15}/cm^2. A similar film which was thermally annealed at 850 °C is shown in (b).

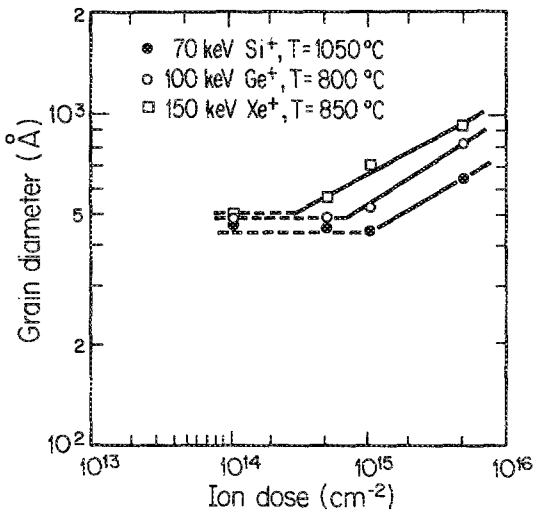

FIG. 26. Variation of grain size with ion dose for 1000 Å Si films.

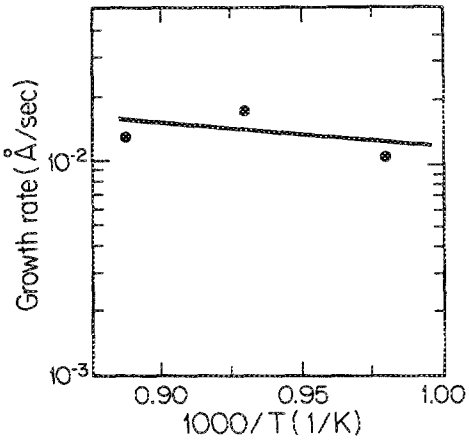

FIG. 28. Arrhenius plot of growth rate of Si, at one half the final grain size, during ion-bombardment-enhanced grain growth with 150 keV Xe^+ ions at a constant current density of 0.3 $\mu A/cm^2$.

of the film introduced some uncertainty in grain size measurements taken in plan view. However, this finding suggests that enhanced grain growth occurs as a result of elastic collisions at or very near grain boundaries, rather than by migration of defects from their points of generation to grain boundaries. If enhanced grain growth occurred via a mechanism in which diffusing point defects enhanced the grain-boundary mobility, we would expect to see enhanced grain growth within a region whose size is determined by the characteristic defect diffusion length, and not simply the size of the damage distribution. An unimplanted Si film also annealed at 850 °C is shown in the cross-sectional electron micrograph of Fig. 25(b) for comparison.

The time dependence for IBEGG in 1000-Å-thick Si films is shown in Fig. 26. Data are shown for IBEGG with 70 keV Si^+ at 1050 °C, 100 keV Ge^+ at 800 °C, and 150 keV Xe^+ at 850 °C. IBEGG is apparent only for ion doses above approximately $1\times10^{15}/cm^2$. This implies that the IBEGG process is less efficient in Si than in Ge or Au films. The slope of the curves indicate that $r\propto t^{0.47-0.51}$, which is consistent with the results for Ge and Au.

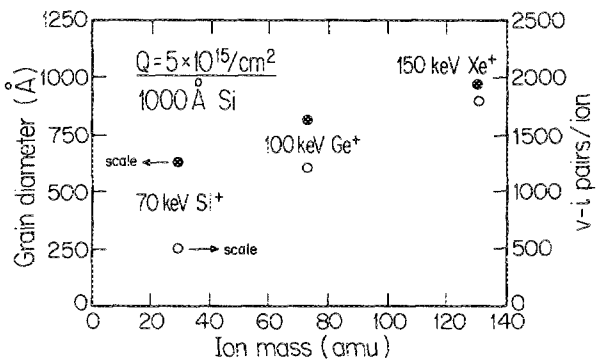

FIG. 27. Comparison of grain size and the number of defects generated per incident ion with projectile ion mass during IBEGG in 1000 Å Si films at 850 °C. The ion dose was $5\times10^{15}/cm^2$ for all cases. Closed circles refer to the left ordinate, and open circles refer to the right ordinate.

The rate of grain growth is proportional to the incident ion mass in a way similar to that seen in Ge and Au films, as shown in Fig. 26. Figure 27 shows the dependence of grain size on incident ion mass for 1000-Å-thick Si films bombarded with Si^+, Ge^+, and Xe^+. Also shown is the yield of beam-generated defects per incident ion, which correlates well with grain size.

The dependence of grain growth rates on temperature is shown in Fig. 28 for Si films bombarded with a current density of 0.3 $\mu A/cm^2$ between 750 and 850 °C. The results suggest that the activation energy for the rate-limiting step in grain-boundary migration is approximately 0.1 eV. This is similar to the activation energy seen in Ge, and is much smaller than the activation energy of 1.3 eV reported for thermal grain growth in intrinsic polycrystalline Si.[18]

IV. A MODEL FOR ION-BOMBARDMENT-ENHANCED GRAIN GROWTH

A. Assumptions

We now describe a simple model for ion-bombardment-enhanced boundary motion. Three assumptions are made about the IBEGG process which are based on experimental observations. The first assumption is that *heating of the film by inelastic collisions, such as those due to electronic stopping and phonon production, are not important for enhanced grain growth.* As discussed earlier, the results shown in Figs. 22 and 23 for Au and in Fig. 25 for Si indicate that beam heating had a negligible effect during these experiments, and did not result in grain growth from thermal annealing. In both cases, the transition region between the bombarded region and the small-grained unbombarded region corresponds to the calculated lateral straggle of the ion beam. Clearly, if grain growth had resulted from a thermal anneal produced by ion beam heating, such a sharp delineation of regions would not be possible.

The second assumption is that *during normal grain growth to a columnar structure, ion bombardment has a negligible influence on the driving force grain growth.* That is, the driving force during IBEGG is similar to the driving force during thermal annealing.

If the driving force were altered by ion bombardment, it is probable that the final thermodynamic state of the film, or the form of evolution to the final state would be different (and would be reflected by a modification of the crystallographic and morphological properties of the film). However, our experimental evidence indicates that (1) the form of the time dependence for grain growth, and (2) the final average grain size, shape of the grain size distribution, distribution of orientations, and morphology are essentially unchanged from their characteristic values during thermally induced grain growth. This suggests that the driving force during IBEGG is similar to the driving force present during thermally induced grain growth. Liu, Nastasi, and Mayer[6] have proposed a model in which the difference in point defect densities of adjacent grains could alter the driving force for grain-boundary motion. Such a difference in defect density might conceivably arise as a result of ion channeling along the high-symmetry crystallographic directions in certain well-oriented grains. However, it is expected that if this situation occurred the film would develop a strong crystallographic texture, which is not observed.

It should be noted that, in the absence of ion bombardment, a preferred crystallographic texture can develop in polycrystalline films via surface-energy-driven secondary grain growth, a process which follows normal grain growth.[7,12,14] The grain size measurements reported here for Ge and Si were made in a regime where the effect of surface energy anisotropy is negligible compared to the grain-boundary energy. Hence, no preferred crystallographic texture was observed as a result of IBEGG in any of the Ge and Si films. In thin Au films, however, the grain size measurements were made in a regime in which the effects surface energy anisotropy are not negligible. A tendency for (111) texture is observed in Au films, which is consistent with the film texture observed as a result of surface-energy-driven secondary grain growth during thermal annealing.[12] It is noteworthy that the most favorable direction for ion channeling in Au is instead the (110) direction. During IBEGG in Au films, the grain size distribution is monomodal and its mean value increases with ion dose, characteristic of normal grain growth.

The development of grain-boundary grooves, illustrated by Fig. 16, might affect the rate of grain-boundary motion during IBEGG. Grooves can impede grain growth in a columnar film.[11] In order to continue grain growth in a grooved film, grain boundaries must either move beyond grooves, which requires an increase in grain-boundary energy, or move with the groove, which requires considerable mass transport. However, in a noncolumnar film, only a few grain boundaries intersect free surfaces. Hence, only these grain boundaries have thermal grooves associated with them. It is worthwhile noting that we do not expect ion bombardment to enhance the rate of grain-boundary grooving via surface diffusion beyond its thermal equilibrium rate, because the ion damage distribution in these experiments was confined to the subsurface region.

Thus, if grain-boundary energy is unaffected by ion bombardment, the total driving force is thought to be unaffected by the IBEGG process in noncolumnar films. As the film becomes more columnar, surface energy and thermal grooving may have more significant effects on IBEGG.

The third assumption is that *only elastic collisions at or very near grain boundaries lead to enhanced grain growth.* This assumption is founded on experimental observations of the temperature dependence and the time dependence of IBEGG compared with thermally induced grain growth.

1. Temperature dependence

The observed temperature dependencies for IBEGG in thin films indicate an activation energy for grain-boundary motion of 0.15 eV for Ge and approximately 0.1 eV for Si. These activation energies are lower than measured and calculated energies of vacancy formation or migration in crystalline Si and Ge,[28,30] although these parameters have not been accurately measured. Less is known about the kinetics of self-interstitials, although it has been suggested that interstitials can migrate essentially athermally in Si.[31] Since the measured activation energies for grain-boundary migration during bombardment are small, but nonzero, it is assumed that thermally induced migration of bombardment-generated defects within the interior of a grain is not the rate-limiting step in grain-boundary migration during IBEGG. This said, it is nevertheless true that defects are created in the interior of each grain in the film. These defects presumably do migrate along defect concentration gradients. It seems plausible that the defects created within grains are responsible for the migration of dislocations which must occur in order to achieve the observed reduction in dislocation and stacking fault densities. In brief, although point defect creation and migration occur, it is proposed that the defects that participate in IBEGG do not migrate through the bulk of the grain. They are created at or very near the boundary so that thermal migration of defects in the bulk is not the rate-limiting step.

2. Time dependence

Another argument favoring the third assumption can be made based upon the observed time dependence of the grain growth kinetics. For the thin films studied here, the time dependence during thermal and ion bombardment-enhanced grain growth is similar; that is, for

$$r \propto t^n, \tag{3}$$

the time exponent n ranges from 0.25 to 0.5.

Now we can develop simple models for the kinetics of grain growth for two cases: (1) IBEGG in which only collisions at grain boundaries lead to grain growth and (2) IBEGG in which defects that are created throughout the film (within grains as well as near grain boundaries) contribute to grain growth. It is assumed that, in the regime where these models apply, the rate of thermal grain growth is negligible.

In the first case we assume that a spatially uniform ion flux leads to a grain-boundary mobility M_{IBEGG} that is independent of grain radius r. The driving force ΔF in normal grain growth is due to the elimination of grain-boundary area, and is inversely proportional to the average radius of

curvature of the grains[14]:

$$\Delta F = 2(\gamma_{gb}/r) . \tag{4}$$

The growth rate is therefore

$$\frac{dr}{dt} = -M_{IB}\overline{V}\Delta F \tag{5}$$

and

$$r^2 - r_0^2 = M_{IB}\overline{V}4\gamma_{gb}t , \tag{6}$$

where $\overline{V}$ is the atomic volume. This is the same expression that is obtained from a simple model[32] of grain growth, except that the mobility is given by M_{IBEGG} rather than the thermal equilibrium mobility. Departures from the idealized $t^{1/2}$ kinetics are not well understood, but are frequently seen experimentally for thermally induced grain growth. A sharp reduction in growth rate upon development of a columnar grain structure, termed the specimen thickness effect, is often seen and may account for this discrepancy.

In the second case we assume that defects are generated throughout the grain and that they migrate to grain boundaries where they affect the mobility of the boundaries. The grains, which are polyhedral in a noncolumnar film, are assumed to be spherical for simplicity. The characteristic defect diffusion length L_D is assumed to be large compared to the grain size.

$$L_D = \sqrt{D_d\tau_d} \gg r , \tag{7}$$

where D_d is the defect diffusivity and τ_d is the defect lifetime. This assumption has been found experimentally to be valid for crystalline Ge and Si in the temperature range of interest here.[33] The number of defects created within a spherical grain of radius r per unit time is N_d.

$$N_d = G_d \tfrac{4}{3}\pi r^3 , \tag{8}$$

where G_d is the defect generation rate per unit volume. The area of the grain boundary is

$$A = 4\pi r^2 . \tag{9}$$

Hence, the number of defects arriving at the boundary per unit area and per unit time is

$$N_d/A = (G_d/3)r . \tag{10}$$

Since we assumed in this case that the rate-limiting step in boundary motion is the rate of defects arriving at the boundary, the mobility in this case is

$$M_{IB} = KG_d r/3 , \tag{11}$$

where K is constant. Assuming a similar driving force as in the first case, the growth rate would be

$$\frac{dr}{dt} = M_{IB}\overline{V}\Delta F = \frac{2KG_d\overline{V}\gamma_{gb}}{3} . \tag{12}$$

The change of grain size r with time is

$$r = 2KG_d\overline{V}\gamma_{gb}t/3 . \tag{13}$$

Thus in this case we predict a linear time dependence which differs more markedly from the IBEGG data than the $t^{1/2}$ time dependence predicted in case (1). The IBEGG data depart from the case (1) time dependence in a manner similar to that of experimental data for thermal grain growth. Although the reasons for the discrepancy are not known, the data are consistent with other experimental investigations of normal grain growth, as mentioned earlier. Hence, the observed time dependence for IBEGG is consistent with case (1) and not the second case.

B. Defect generation rate

The rate of generation of beam-produced point defects can be estimated from known experimental parameters and TRIM calculations. The defect generation rate per substrate atom, $\Delta k_{Gd}(z)$, can be related to the ion beam current density J by

$$\Delta k_{Gd}(z) = J\mathscr{R}(z)/qN_l , \tag{14}$$

where q is electronic charge and N_l is the lattice atomic density. The quantity $\mathscr{R}(z)$ is the number of beam-generated defects/ion cm. The z direction denotes distance into the film. The damage profile $\mathscr{R}(z)$ is usually qualitatively similar to the range profile of the implanted ions. The total defect yield/ion, $\overline{R}$, is the parameter calculated by the TRIM program,

$$\overline{R} = \int_0^h \mathscr{R}(z)dz, \tag{15}$$

where h denotes film thickness. If the beam generated defect profile varies slowly through the film thickness, then the defect yield/ion cm can be approximated as

$$\mathscr{R}(z) \simeq \overline{R}/h . \tag{16}$$

Since all the grain size measurements are made from transmission electron micrographs taken in plan view, small variations in $\mathscr{R}$ with depth in the film should not severely affect correlations with grain size measurements, so this approximation seems reasonable. The defect generation rate therefore becomes, in units of defects/atom s,

$$\Delta k_{Gd} = J\overline{R}/qN_l h . \tag{17}$$

C. A transition state model for IBEGG kinetics

We now develop a simple expression based on rate theory for normal gain growth kinetics during ion bombardment. This analysis extends a model outlined earlier.[34]

The average rate of boundary motion can be expressed as a sum of terms corresponding to n possible processes,[34]

$$\frac{dr}{dt} = \lambda \sum_{j=1}^{n} \Delta k_j , \tag{18}$$

where λ is the average jump distance and Δk_j is the net forward jump rate at the boundary for the jth process. Each jump rate can be thought of as an independent bimolecular process consisting of (a) formation of a vacant site into which an atom can jump and (b) an atomic jump across the boundary into the vacant site. Each process has a net jump rate

$$\Delta k_j = \mathscr{P} k_{jump_j} , \tag{19}$$

where $\mathscr{P}$ is the probability that a vacant site is available and Δk_{jump_j} is the net jump rate given that a vacant site is available. In principle, each of these steps can be due either to a thermal or a collision-induced event. Following Turnbull,[32]

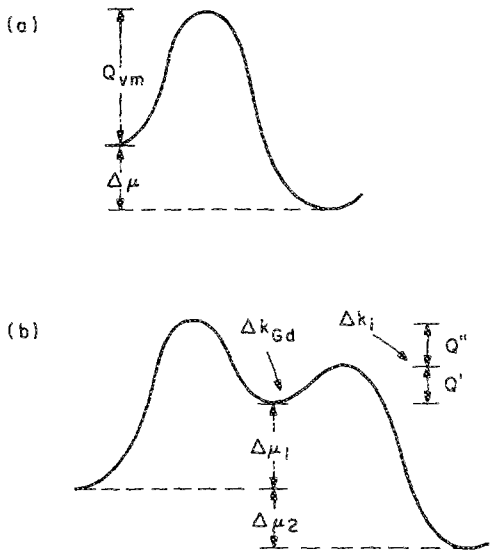

FIG. 29. Schematic depicting thermal jumps across an energy barrier with energy Q.

the rate of boundary migration can also be expressed as

$$\frac{dr}{dt} = -\sum_{j=1}^{n} M_j \bar{V} \Delta F, \tag{20}$$

where M_j is the grain-boundary mobility for the jth process during ion bombardment, $\bar{V}$ is the atomic volume, and ΔF is the driving force for boundary motion.

Figure 29(a) depicts purely thermally induced jumps across an energy barrier with height Q_{vm}. A schematic diagram for this event is shown in Fig. 30. In the case of thermally induced grain growth, both the atomic migration event and the vacant site formation event are due to thermal processes. For thermally induced grain growth, the net number of jumps per unit time across a grain boundary in the forward direction Δk_1 is

$$\Delta k_1 = k_+ - k_-, \tag{21}$$

where $k_+ = k_0 e^{(-Q_{vm}/kT)}$ and $k_- = k_0 e^{-(Q_{vm}+\Delta\mu)/kT}$. If we define the energy for formation of a vacant boundary site to be Q_{vf}, the probability of a vacant final site is $e^{-Q_{vf}/kT}$. Hence Δk is related to the chemical potential $\Delta\mu$ by

$$\Delta k_1 = k_0 e^{-(Q/kT)}(1 - e^{-\Delta\mu/kT}), \tag{22}$$

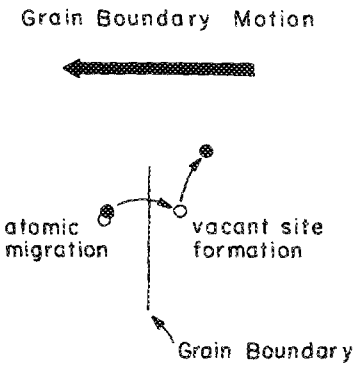

FIG. 30. Schematic depicting a general bimolecular process for grain-boundary motion during ion bombardment. Both the atomic migration event and the vacant site event can be limited by thermal processes or by ion bombardment.

where $Q = Q_{vm} + Q_{vf}$. This result is consistent with the expression found by Turnbull[32] for thermally induced boundary migration, although here we have modeled grain growth as a bimolecular process. The chemical potential is related to the driving force by

$$\Delta\mu = \Delta F \bar{V}/N, \tag{23}$$

where N is Avogadro's number and $\bar{V}$ is the atomic volume. The rate of grain-boundary motion is then

$$\frac{dr}{dt} = \lambda \Delta k_1, \tag{24}$$

where λ is the jump distance. For $\Delta F \bar{V} \ll NkT$,

$$\frac{dr}{dt} = -\frac{\lambda}{RT} k_0 e^{-Q/kT}(\bar{V}\Delta F), \tag{25}$$

where $R = Nk$. The quantity k_0 can be related to a diffusivity D_0 (Ref. 32) by

$$k_0 = D_0/\lambda^2, \tag{26}$$

so

$$\frac{dr}{dt} = -\frac{D_0 \bar{V}}{\lambda RT} e^{-Q/kT} \Delta F, \tag{27}$$

or, written in terms of the mobility,

$$\frac{dr}{dt} = -M_1 \bar{V} \Delta F, \tag{28}$$

where the thermal mobility is

$$M_1 = (D_0/\lambda RT) e^{-Q/kT}. \tag{29}$$

There are several possible combinations of the atomic migration and vacant site formation events depicted in Fig. 30 which can result in bombardment-enhanced grain-boundary motion: one process, which we will label process 2, in which a vacant site is created at the boundary by ion bombardment, and migration of the vacant site occurs due to a thermal process; another process, process 3, in which thermally induced vacant site formation occurs at the boundary and is accompanied by motion of a collision-induced interstitial into the vacant site; and process 4 which involves motion of a collision-induced interstitial to a collision-induced vacant site at the boundary.

For process 2, the net rate of forward jumps across the boundary is

$$\Delta k_2 = (\Delta k_{Gd} \tau)\left[k_0 e^{-Q_{vm}/kT}(1 - e^{-\Delta\mu/kT})\right], \tag{30}$$

where Δk_{Gd} is the generation rate of collision-induced defects at the boundary, and τ is the lifetime of such a defect. If process 2 dominates during grain-boundary motion, the grain growth rate is

$$\frac{dr}{dt} = \Delta k_{Gd} \tau \frac{D_0 \bar{V}}{\lambda RT} e^{-Q_{vm}/kT} \Delta F. \tag{31}$$

In processes 3 and 4, we assume that bombardment leads to atomic jumps into intermediate interstitial states at the boundary with rate Δk_{Gd}, as illustrated in Fig. 29(b). The net rate of forward jumps out of the intermediate state is Δk_i, and the activation energy for forward jumps is Q'. Structural models of high-angle grain boundaries in the diamond cubic lattice suggest possible locations for this intermediate state.[35,36] For many orientations, it is possible to

generate a structure with boundary interstitial sites which have greater volume than the bulk interstitial site. The net jump rate for process 3 is

$$\Delta k_3 = (e^{-Q_{vf}/kT})\left(\frac{\Delta k_{Gd}\,\Delta k_i}{\Delta k_{Gd} + \Delta k_i}\right), \tag{32}$$

where Δk_i is the net jump rate in the forward direction from the intermediate state, and is given by

$$\Delta k_i = k_0 e^{-Q'/kT}[(1 - e^{-(\Delta\mu_1 + \Delta\mu_2)/kT}) - e^{-Q''/kT}(1 - e^{-\Delta\mu_1/kT})]\,. \tag{33}$$

For the case in which $\Delta k_{Gd} \gg k_i$, and when ΔF_1 and ΔF_2 are much less than RT, the grain growth rate is

$$\frac{dr}{dt} = e^{-(Q_{vf}+Q')/kT}\frac{D_0\overline{V}}{\lambda RT}[(1 - e^{-Q''/kT})\Delta F_1 + \Delta F_2]\,, \tag{34}$$

where ΔF_1 and ΔF_2 are the driving forces corresponding to the changes in chemical potential $\Delta\mu_1$ and $\Delta\mu_2$. If $\Delta k_{Gd} \ll k_i$, then

$$\frac{dr}{dt} = \lambda e^{-Q_{vf}/kT}\Delta k_{Gd}\,. \tag{35}$$

We believe that process 3 is unlikely to describe boundary motion during bombardment, since the activation energy for grain-boundary motion by process 3 is at least equal to the energy of thermal vacancy formation at the boundary. The activation energy for vacant site formation at the boundary is probably similar to the energy for bulk vacancy formation. Also, the thermally induced vacancy population is smaller than the collision-induced defect population in the regime of our experiments.

Process 4 involves collision-induced formation of both vacancies and interstitials. The net rate of forward jumps is

$$\Delta k_4 = (\Delta k_{Gd}\tau)\left(\frac{\Delta k_{Gd}\,\Delta k_i}{\Delta k_{Gd} + \Delta k_i}\right). \tag{36}$$

There are two limiting cases for boundary motion in process 4. In the first case, when $\Delta k_i \ll \Delta k_{Gd}$, the activation energy is equal to the energy of migration out of the intermediate state Q' and $\Delta k_4 \propto \Delta k_{Gd}$. For this case, the rate of grain-boundary motion is

$$\frac{dr}{dt} = \Delta k_{Gd}\tau\, e^{-Q'/kT}\frac{D_0\overline{V}}{\lambda RT}[1 - e^{-Q''/kT})\Delta F_1 + \Delta F_2]\,. \tag{37}$$

In the second case, when $\Delta k_i \gg \Delta k_{Gd}$, the rate of grain-boundary motion is

$$\frac{dr}{dt} = \Delta k_{Gd}^2\tau\,. \tag{38}$$

This latter case implies that the activation energy is zero, and $dr/dt \propto \Delta k_{Gd}^2$; that is, that the rate of grain-boundary motion is expected to exhibit a *second-order dependence on the rate of collision-induced defect formation*, and hence also the ion beam current density. Based on our measurements of the dependence of grain growth on the concentration of collision-induced defects, which were not extensive, bombardment-enhanced grain growth appears to exhibit a first-order dependence on the rate of collision-induced defect formation, arguing against the latter limiting case for process 4.

TABLE I. Values for number of jumps at a grain boundary per defect generated for various 500 Å Ge films.

Projectile ion	Substrate	Temp. (°C)	$\overline{R}$	$\mathscr{C}$
50 keV Ge	500 Å Ge, freestanding, am-dep	600	1131	2.5
50 keV Ge	500 Å Ge, freestanding, am-dep	500	1131	2.7
50 keV Ge	500 Å Ge/SiO_2, am-dep	600	1131	1.1
50 keV Ge	500 Å Ge/SiO_2, am-dep	500	1131	1.3
50 keV Ge	500 Å Ge/SiO_2, poly-dep	500	1131	1.7
50 keV Ge	500 Å Ge/SiO_2, poly-dep	600	1131	1.7
50 keV Ar	500 Å Ge/SiO_2, am-dep	600	762	1.7
50 keV Kr	500 Å Ge/SiO_2, am-dep	600	983	1.7
100 keV Xe	500 Å Ge/SiO_2, am-dep	600	2104	1.6

Both process 2 and the former limiting case for process 4 are consistent with a first-order dependence on Δk_{Gd}, and also a weak (but nonzero) temperature dependence. Our experimental results do not allow us to distinguish between these processes. Therefore, we believe that the dominant process in bombardment-enhanced grain growth is either process 2 or process 4 in the limit where the jump out of an intermediate boundary site is rate limiting.

V. ATOMIC JUMP RATE AT THE BOUNDARY

It is interesting to consider the atomic jump rate at the boundary during IBEGG from a microscopic viewpoint. An idealized one-dimensional grain boundary which spans the film thickness has a velocity $\Delta r/\Delta t$ given by

$$\Delta r/\Delta t = \lambda\Delta k, \tag{39}$$

where λ is the jump distance and Δk is the net rate of jumps in the forward direction, as before. The generation rate is assumed to be related to Δk by

$$\Delta k = \mathscr{C}\,\Delta k_{Gd} = \mathscr{C}\,(J\overline{R}/q\,N_l h)\,. \tag{40}$$

For the moment, the weak IBEGG temperature dependence is ignored. The velocity is then

$$\Delta r/\Delta t = \lambda\mathscr{C}\,(J\overline{R}/q\,N_l h)\,. \tag{41}$$

The coefficient $\mathscr{C}$ is the number of atomic jumps at the boundary per defect generated at the boundary

$$\mathscr{C} = \Delta r N_l h/\lambda Q_d R\,, \tag{42}$$

where the ion dose $Q_d = J\Delta t/q$ and Δt denotes the time of

TABLE II. Values for number of jumps at a grain boundary per defect generated for various 250 Å Au films.

Projectile ion	Substrate	Temp. (°C)	$\overline{R}$	$\mathscr{C}$
40 keV Kr	250 Å Au, freestanding	23	608	4.1
60 keV Kr	250 Å Au, freestanding	23	890	4.0
80 keV Kr	250 Å Au, freestanding	23	1175	5.9
100 keV Kr	250 Å Au, freestanding	23	1421	7.4
60 keV Ar	250 Å Au, freestanding	23	703	7.3
200 keV Xe	250 Å Au, freestanding	23	2681	5.2

TABLE III. Values for number of jumps at a grain boundary per defect generated for various 1000-Å-thick Si films.

Projectile ion	Substrate	Temp. (°C)	$\bar{R}$	$\mathscr{C}$
70 keV Si	1000 Å Si/SiO_2	1050	450	1.5
100 keV Ge	1000 Å Si/SiO_2	800	1141	1.4
150 keV Xe	1000 Å Si/SiO_2	850	1810	1.3

bombardment. The variation of Δr with Q_d has been measured and values for $\bar{R}$ have been calculated with TRIM. The values for $\mathscr{C}$ have been computed for various 500 Å Ge films in Table I. The driving force was assumed to be a function only of grain size, not the microstructural topology of the film. In each case, the number if jumps/defect is in the range of 1–2.5. It is interesting to note that $\mathscr{C}$ is roughly constant, even though $\bar{R}$ varied widely. Also the value $\mathscr{C} \approx 1$ is a physically plausible number in terms of the linear collision cascade model of defect generation, which assumes binary collision between ions or recoils and target atoms.

Similar data are shown in Table II for 250 Å Au films under different IBEGG conditions. The value of $\mathscr{C}$ is higher for Au, which may be an indication that the driving force, due to reduction of grain-boundary energy, is different for Au than for Ge.

In Table III, data are given for $\mathscr{C}$ for Si films. As before, the grain-boundary energy in Si is assumed to be similar to that in Au and Ge. The values of $\mathscr{C}$ are somewhat lower than the corresponding numbers for Ge and Au films. Again, it is difficult to determine whether this reflects a difference in IBEGG mechanism or is due to the approximation of the driving force and jump distance. Nonetheless, the values of $\mathscr{C}$ are similar, even though $\bar{R}$ varied widely.

VI. COMPARISON OF THERMAL AND IBEGG DEFECT CONCENTRATIONS

It is also interesting to compare the concentration of vacancy-interstitial pairs generated during IBEGG with the concentration of defects that exists at thermal equilibrium at a given temperature. If the entropy of vacancy formation is assumed to be small, the thermal equilibrium concentration of vacancies n_{te}, is

$$n_{te} \simeq N_l \exp - (H_{vf}/kT) , \tag{43}$$

where H_{vf} is the enthalpy of vacancy formation. For Ge, H_{vf} is approximately 1.9 eV.[30] The IBEGG defect concentration, n_{IBEGG}, can be approximated as

$$n_{\mathrm{IBEGG}} \simeq J\bar{R}\tau/2qh , \tag{44}$$

where τ is the vacancy-interstitial pair lifetime.

For the case of the IBEGG data given in Fig. 13, $J = 0.25\,\mu\mathrm{A/cm^2}$, $R = 1194$, and τ is estimated to be 0.1 μs, based on the vacancy diffusivity given in Ref. 30, and assuming a diffusion length of approximately 600 Å in the Ge thin film. In this case $n_{\mathrm{IBEGG}} = 1.9 \times 10^{13}/\mathrm{cm^3}$. This is equal to the estimated thermal equilibrium defect concentration at $T = 750$ °C. Referring again to Fig. 13, it is seen that the intersection of the two curves, i.e., the temperature at which the measured growth rates for thermal annealing and IBEGG are equal, is approximately 710 °C. This may be an indication that the grain growth rate is proportional to the concentration of point defects at or very close to the boundary in both cases.

VII. SUMMARY

We have studied ion-bombardment-enhanced grain growth in thin films of Ge, Au, and Si. The grain growth rate during ion bombardment is weakly temperature dependent and is proportional to the energy deposited in elastic collisions at or very near grain boundaries. The number of atomic jumps per defect generated at the boundary was found to be approximately constant and characteristic for each material. A transition state model has been developed which suggests that bombardment-enhanced grain growth may be due to thermal migration of bombardment-generated defects across the boundary. Comparison of the rates of thermally induced and bombardment-enhanced grain growth in Ge suggest that boundary motion is proportional to the defect concentration at the boundary, regardless of whether they are generated thermally or by an ion bombardment.

ACKNOWLEDGMENTS

It is a pleasure to acknowledge the expert assistance of M. McAleese and J. Woodhouse of the MIT Lincoln Laboratory. This research was sponsored by the National Science Foundation and the Air Force Office of Scientific Research.

[1] P. Wang, D. A. Thompson, and W. W. Smeltzer, Nucl. Instrum. Methods B **7/8**, 97 (1986).
[2] P. Wang, D. A. Thompson, and W. W. Smeltzer, Nucl. Instrum. Methods B **16**, 288 (1986).
[3] J. C. Liu and J. W. Mayer, Nucl. Instrum. Methods B **19/20**, 538 (1987).
[4] H. A. Atwater, H. I. Smith, and C. V. Thompson, in *Beam-Solid Interactions and Phase Transformations*, edited by H. Kurz, G. L. Olson, and J. M. Poate (Materials Research Society, Pittsburgh, PA, 1986), Vol. 51, pp. 337–342.
[5] H. A. Atwater, C. V. Thompson, and H. I. Smith, in *Beam-Solid Interactions and Transient Processes*, edited by S. T. Picraux, M. O. Thompson, and J. S. Williams (Materials Research Society, Pittsburgh, PA, 1987), Vol. 74, pp. 499–504.
[6] J. C. Liu, M. Nastasi, and J. W. Mayer, J. Appl. Phys. **62**, 423 (1987).
[7] J. E. Palmer, S.M. thesis, MIT, 1985; J. E. Palmer, C. V.Thompson, and H. I. Smith, J. Appl. Phys. **62**, 2492 (1987).
[8] P. Feltham, Acta Metall. **5**, 97 (1957).
[9] M. Hillert, Acta Metall. **13**, 227 (1965).
[10] N. P. Louat, Acta Metall. **22**, 721 (1974).
[11] W. W. Mullins, J. Appl. Phys. **28**, 333 (1957).
[12] C. C. Wong, Ph.D. thesis, MIT, 1986; C. C. Wong, H. I. Smith, and C. V. Thompson, Appl. Phys. Lett. **48**, 335 (1986).
[13] H-J. Kim and C. V. Thompson, Appl. Phys. Lett. **48**, 399 (1986).
[14] C. V. Thompson, J. Appl. Phys. **58**, 763 (1985).
[15] J. R. Vig, J. Vac. Sci. Technol. A **3**, 1027 (1985).
[16] Y. Wada and S. Nishimatsu, J. Electrochem. Soc. **125**, 1499 (1978).
[17] L. Mei, M. Rivier, Y. Kwark, and R. W. Dutton, J. Electrochem. Soc. **129**, 1791 (1982).
[18] H-J. Kim and C. V. Thompson, in *Polysilicon Films and Interfaces*, edited by C. Y. Wong, C. V. Thompson, and K-N. Tu (Materials Research Society, Pittsburgh, PA, 1988), Vol. 106.
[19] J. P. Biersack and L. G. Haggmark, Nucl. Instrum. Methods **174**, 257 (1980).
[20] M. J. Norgett, M. T. Robinson, and I. M. Torrens, Nucl. Eng. Design **33**, 50 (1974).
[21] J. F. Ziegler, J. P. Biersack, and U. Littmark, *The Stopping and Range of Ions in Solids* (Pergamon, New York, 1986).

[22]D. A. Thompson, Radiat. Effects **56**, 105 (1981).
[23]G. F. Bolling and W. C. Winegard, Acta Metall. **6**, 283 (1958).
[24]P. Gordon and T. A. El-Bassyouni, Trans. AMIE **233**, 391 (1965).
[25]S. K. Dutta and R. M. Spriggs, J. Am. Ceram. Soc. **53**, 61 (1970).
[26]R. S. Gordon, D. D. Marchant, and G. W. Hollenberg, J. Am. Ceram. Soc. **53**, 399 (1970).
[27]A. Seeger and K. P. Chik, Phys. Status Solidi **29**, 455 (1968).
[28]J. A. Van Vechten, Phys. Rev. B **10**, 1482 (1974).
[29]G. N. Van Wyk and H. J. Smith, Nucl. Instrum. Methods **170**, 433 (1980).
[30]K. H. Bennemann, Phys. Rev. **130**, 1763 (1963).
[31]G. D. Watkins, in *Radiation Damage in Semiconductors* (Dunod, Paris, 1965), p. 97; G. D. Watkins, J. Phys. Soc. Jpn. **18**, Suppl. II, 22 (1963).
[32]D. Turnbull, Trans. AIME **191**, 661 (1951).
[33]R. L. Minear, D. G. Nelson, and J. F. Gibbons, J. Appl. Phys. **43**, 3468 (1972).
[34]H. A. Atwater, C. V. Thompson, and H. I. Smith, Phys. Rev. Lett. **60**, 112 (1988).
[35]J. Hornstra, Physica **25**, 409 (1959).
[36]J. T. Wetzel, A. A. Levi, and D. A. Smith, in *Grain Boundary Structure and Related Phenomena*, edited by Y. Ishida, Japan Institute of Metals International Symposium (Japan Institute of Metals, Miyagi, 1986), Vol. 4, pp. 1061–1067.